Eur. Phys. J. A (2012) **48**: 14
DOI 10.1140/epja/i2012-12014-9

THE EUROPEAN PHYSICAL JOURNAL A

Regular Article – Experimental Physics

Exclusive electroproduction of $K^+\Lambda$ and $K^+\Sigma^0$ final states at $Q^2 = 0.030$–0.055 (GeV/c)^2

A1 Collaboration

P. Achenbach[1,a], C. Ayerbe Gayoso[1], J.C. Bernauer[1,b], S. Bianchin[2], R. Böhm[1], O. Borodina[2], D. Bosnar[3], M. Bösz[1], V. Bozkurt[2], P. Bydžovský[4], L. Debenjak[5], M.O. Distler[1], A. Esser[1], I. Friščić[3], M. Gómez Rodríguez[1], B. Göküzüm[2], K. Grießinger[1], P. Jennewein[1], E. Kim[2], M. Makek[3], H. Merkel[1], S. Minami[2], U. Müller[1], D. Nakajima[2], L. Nungesser[1], B. Özel-Tashenov[2], J. Pochodzalla[1], Ch. Rappold[2], T.R. Saito[1,2], S. Sánchez Majos[1], B.S. Schlimme[1], S. Širca[5], M. Weinriefer[1], and C.J. Yoon[1,c]

[1] Institut für Kernphysik, Johannes Gutenberg-Universität, Mainz, Germany
[2] GSI, Helmholtz Center for Heavy Ion Research, Darmstadt, Germany
[3] Department of Physics, University of Zagreb, Croatia
[4] Nuclear Physics Institute, Řež near Prague, Czech Republic
[5] University of Ljubljana and Jožef Stefan Institute, Ljubljana, Slovenia

Received: 9 November 2011 / Revised: 2 January 2012
Published online: 10 February 2012 –
Communicated by M. Guidal

Abstract. Cross-section measurements of the exclusive $p(e, e'K^+)\Lambda, \Sigma^0$ electroproduction reactions have been performed at the Mainz Microtron MAMI in the A1 spectrometer facility using for the first time the KAOS spectrometer for kaon detection. These processes were studied in a kinematical region not covered by any previous experiment. The nucleon was probed in its third-resonance region with virtual photons of low four-momenta, $Q^2 = 0.030$–$0.055\,(\mathrm{GeV}/c)^2$. The MAMI data indicate a smooth transition in Q^2 from photoproduction to electroproduction cross-sections. Comparison with predictions of effective Lagrangian models based on the isobar approach reveal that strong longitudinal couplings of the virtual photon to the N^* resonances can be excluded from these models. Modern isobar and Regge-plus-resonance models are in agreement with the data.

1 Introduction

The Mainz Microtron MAMI at the Institut für Kernphysik in Mainz is an accelerator to study hadrons with the electromagnetic probe [1]. The exclusive production of mesons by electron and photon beams impinging on liquid-hydrogen targets has been proven to be a valuable tool for investigating the hadronic structure of the nucleon. At the energy scale of the nucleon mass, hadrons are complex systems, whose description by fundamental equations for the dynamics of asymptotically free quarks and gluons is complicated by the non-perturbative nature of QCD. Instead, a successful description of these reactions has been obtained with hadronic field theories. The approach is based on effective degrees of freedom, where mesons and baryons are treated as fundamental objects that interact with one another, characterized by properties such as mass, charge, spin, parity, form factors, and coupling constants. Studies of strange final states provide additional information on the baryonic resonances.

In one particular type of the single-channel model, based on an effective Lagrangian and commonly referred to as the isobar approach, the reaction amplitude is constructed in the lowest-order perturbation theory (tree level) assuming Born terms and exchanges of various nucleon, hyperon, and meson resonances in the s-, u-, and t-channels, respectively. Copious applications of these models into the strangeness sector started in the 1980s, *e.g.*, [2–7].

In the electromagnetic production of kaons on nucleons, the final kaon-hyperon system is coupled with other possible reaction channels, like πN and ηN, via the rescattering of hadrons. This final-state interaction (FSI) is included explicitly in the coupled-channel approaches [8, 9]. However, those models are limited to the reactions with real photons. In general, the electroproduction reaction is well described by the single-channel models. It is supposed

[a] e-mail: patrick@kph.uni-mainz.de
[b] *Present address*: MIT-LNS, Cambridge, MA, USA.
[c] *Present address*: Department of Physics and Astronomy, Seoul National University, Korea.

that part of the FSI effect is absorbed into the values of the model parameters being fitted to data.

Another model for the kaon electroproduction is the Regge-plus-resonance model developed by the Ghent group [10,11]. In their approach, the non-resonant part of the $K^+\Lambda$ production amplitude is described with a Regge model by the exchange of kaonic trajectories in the t-channel. The resonant part of the amplitude is modelled by the s-channel exchanges of a moderate number of nucleon resonances, also assuming an effective Lagrangian [10]. This approach has the advantage of containing fewer parameters.

In the one-photon exchange approximation for electromagnetic scattering of unpolarized electrons off unpolarized target nucleons with coincident kaon detection, the virtual photoproduction cross-section can be expressed as

$$\frac{\mathrm{d}\sigma_v}{\mathrm{d}\Omega_K^{c.m.}} = \sigma_T + \varepsilon\,\sigma_L + \sqrt{2\varepsilon(\varepsilon+1)}\,\sigma_{TL}\cos\phi + \varepsilon\,\sigma_{TT}\cos 2\phi\,, \quad (1)$$

where the terms indexed by T, L, TL, TT are the transverse, longitudinal and interference structure functions that depend on the virtual photon's four-momentum squared Q^2, the hadronic energy W, and the kaon centre-of-mass polar angle $\theta_K^{c.m.}$. The angle ϕ is the angle between the electron-scattering and hadron-production planes. This expression shows the close connection between electro- and photoproduction. At MAMI the transitional region at $Q^2 < 0.5\,(\mathrm{GeV}/c)^2$ is accessible with virtual photons that are polarized with a degree of polarization ε. Longitudinal and longitudinal-transverse interference structure functions are accessible only in electroproduction experiments. Although not necessarily being small, they are suppressed in the total cross-section through a factor Q^2/ω^2, with ω being the photon energy. The σ_{TT} and σ_T structure functions are related to the polarized photon asymmetry Σ, that could be measured in photoproduction experiments with real polarized photons, by the relation $\Sigma = -\sigma_{TT}(Q^2 \to 0)/\sigma_T(Q^2 \to 0)$. The transverse-transverse interference structure function for virtual photons accounts for their partial linear polarization. For real unpolarized photons and unpolarized target nucleons only the transverse structure function remains. With these connections it is instructive to compare the electroproduction cross-section at very low Q^2 directly to unpolarized photoproduction. In this kinematical region, electromagnetic form factors that describe the electromagnetic structure of hadrons are not expected to influence the structure functions too much as they provide a smooth Q^2 dependence near the photoproduction point at $Q^2 = 0$. More pronounced effects at very low momentum transfer can arise from dynamics of the reaction, *e.g.*, couplings of the longitudinal mode of the virtual photon to baryons, which can be studied only in electroproduction.

In order to provide a comprehensive understanding of the elementary kaon production reaction, large kinematic coverage of experimental data on photo- and electroproduction is needed. Although recent photo- and electroproduction measurements with high statistics have been performed at Jefferson Lab [12–16], the region of very low momentum transfers was up to now not covered experimentally. A phenomenological extrapolation of the CLAS data from $Q^2 > 0.65\,(\mathrm{GeV}/c)^2$ to the photoproduction point leads to values of the transverse structure function σ_T systematically larger than the measured values in photoproduction [14]. This unknown transitional region is particularly interesting since predictions of models for the separated cross-sections differ significantly here, see, *e.g.*, fig. 3 in [15]. The goal of the first measurement at MAMI was to probe the elementary reaction at low-momentum transfers and to determine the angular dependence of the electroproduction cross-section in this kinematic region.

2 Experiment

First experiments on the electroproduction of kaons off a liquid-hydrogen target were performed in Mainz with an unpolarized electron beam of 1.508 GeV energy in the years 2008–2009. The liquid-hydrogen target cell was 11 mm wide and 48 mm long with walls made of 10 μm thick havar foil. A current of 1–4 μA was rastered with a few kHz in the transverse directions with an amplitude of ± 5 mm in order to avoid local boiling of the liquid. The scattered electrons from the $p(e, e'K^+)$ reaction were detected in SpekB, one of the high-resolution magnetic spectrometers of the A1 Collaboration's spectrometer facility [17], and the positive kaons in the Kaos spectrometer [18]. With its very compact design and a length of the central trajectory of only 5.3 m to the focal plane, the Kaos spectrometer complements the facility in reactions with open strangeness.

The electron arm central momentum was 0.33 GeV/c during part of the 2008 beam time and throughout the 2009 beam time, while it was 0.45 GeV/c during one dedicated study of the $K^+\Lambda$ channel in 2008. In both experimental settings the central momentum for the kaon arm was 0.53 GeV/c. The central spectrometer angle of the kaon arm was 31.5° with a large angular acceptance in the dispersive plane of $\theta_K^{lab} = 21$–43°. The electron spectrometer was fixed at the minimum forward angle of $\theta_{e'}^{lab} \approx 15°$, thereby maximising the virtual photon flux. The coverage of the photon's four-momenta was $Q^2 = 0.030$–$0.055\,(\mathrm{GeV}/c)^2$ with central values of $Q^2 = 0.036$ and $0.050\,(\mathrm{GeV}/c)^2$ for the two kinematic settings. The corresponding degrees of polarization were $\varepsilon = 0.4$ and 0.54. Photon energies, ω, were near the maximum of the kaon production cross-section at 1.18 GeV and 1.04 GeV, exciting the hadronic system to invariant energies $W = 1.75$ GeV and 1.67 GeV.

Track determination is performed in SpekB by means of two vertical drift chambers, and timing and trigger signals are provided by two segmented planes of plastic scintillators immediately behind. A gas-filled threshold Cherenkov detector is operated to provide a good separation between pions and electrons. To perform clean electron identification, a signal in the Cherenkov counter was required. SpekB reaches a momentum resolution (FWHM)

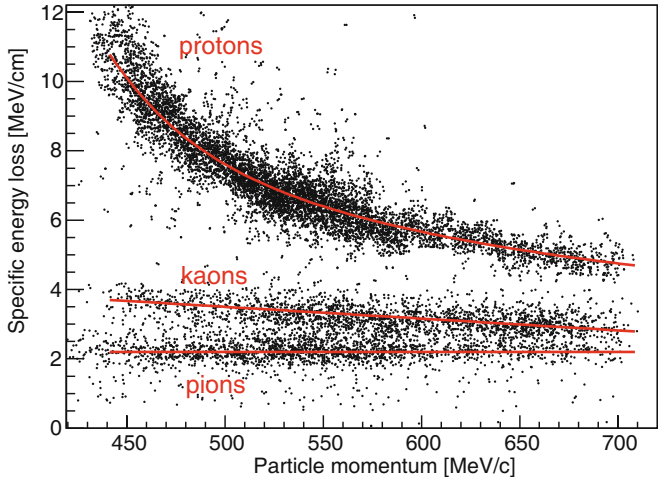

Fig. 1. Measured energy deposition per unit path length in one scintillator wall as a function of momentum after particle identification cuts. Lines for the expected rate of energy losses for pions, kaons, and protons are shown.

of $\delta p/p < 10^{-4}$ and an angular resolution of better than 0.2 mrad.

In the KAOS spectrometer's hadron arm there are two segmented scintillator walls with 30 paddles each serving as timing, energy loss, and trigger detectors. Two multi-wire proportional chambers serve as coordinate detectors near the focal plane. A dedicated set of efficiency counters was built to measure tracking efficiencies for the abundant pions and protons. The relatively large overlap between the liberated charges for these two particle species was used to extract the tracking efficiency for kaons.

The intrinsic efficiency of a single MWPC was measured to be better than 98%. Track reconstruction efficiencies were dependent on beam intensity, being 75–90% at beam currents of 1–4 μA [19]. To identify kaons in the measured range of momenta from 0.4 to 0.7 GeV/c, their energy deposition in the scintillators and coincidence time were used. The signal amplitudes from the individual paddles were corrected for the reconstructed path length through the scintillator bulk material and the light absorption inside. See fig. 1 for the measured specific energy loss in one scintillator wall as a function of momentum after particle identification cuts. The energy deposition per unit path length corrected for the expected kaon rate of energy loss, ΔE^K, was required to be within $|\Delta E^K| < 640$ keV. The fraction of kaons lost in this cut was calculated from Gaussian functions plus a constant background that were fitted to the specific energy loss distributions in small bins of limited momentum acceptance. The cut condition corresponds to a 2σ width around the expected kaon rate of energy loss. The coincidence time spectra after particle identification cuts for the $p(e,e'K^+)$ and $p(e,e'\pi^+)$ reactions are shown in fig. 2, where the coincidence time was determined by using the reconstructed momentum and path length under the assumption that a kaon or pion was detected. After correction of the coincidence time for the flight path lengths, an overall time-of-flight resolution

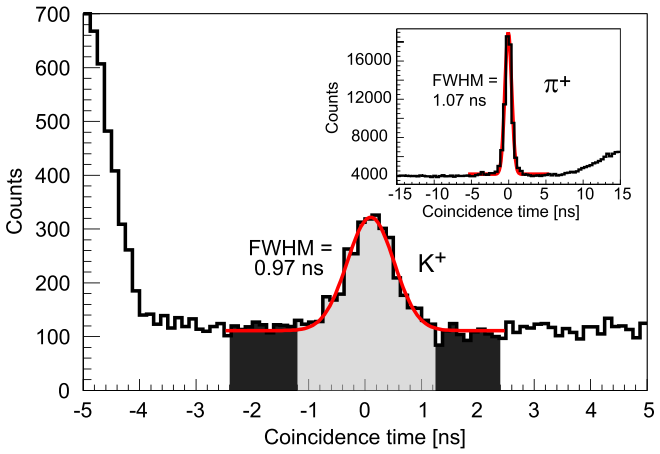

Fig. 2. Coincidence time spectra for the $p(e,e'K^+)$ reaction as well as for the dominant $p(e,e'\pi^+)$ reaction (insert), after corrections for the reconstructed flight path length and particle identification cuts. Gaussian distributions on top of a constant background were fitted to the spectra. The width of the (e',π^+) peak is $\Delta t_{\mathrm{FWHM}} = 1.07$ ns, the width of the (e',K^+) peak is $\Delta t_{\mathrm{FWHM}} = 0.97$ ns. The cut regions for selecting true and random coincidences of kaons are indicated by shades of grey.

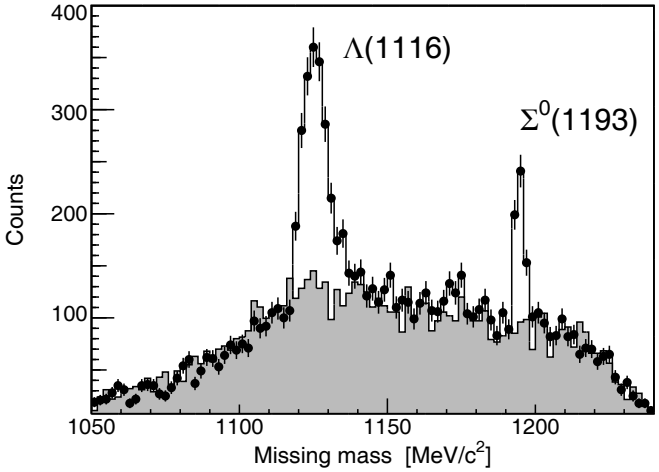

Fig. 3. Missing mass spectrum in the $p(e,e'K^+)\Lambda,\Sigma^0$ reaction for one data set. The shaded histogram shows the missing mass distribution in two averaged (e',K^+) coincidence time sidebands with the appropriate weights and $\sim 10\%$ of coincident background.

of $\Delta t_{\mathrm{FWHM}} \approx 1$ ns was achieved. The flight time difference to the expected kaon flight time, Δt^K, was required to be within $|\Delta t^K| < 1.2$ ns. The hadron arm trigger was generated by a combination of the hits in the two scintillator walls. Since the KAOS spectrometer was operated as a single dipole with open yoke geometry, a study was performed on the contributions from coincident particles originating outside the spectrometer acceptance that scattered into the detectors. These type of events were eliminated by the tracking cuts.

The measured momenta of the kaon and the electron allow for a full reconstruction of the missing energy and missing momentum of the recoiling system. The missing

mass spectrum of one data set is shown in fig. 3 with the mass resolution being sufficient to clearly separate Λ from Σ hyperons as the unobserved baryon in the reaction. Random background events, identified by two averaged (e', K^+) coincidence time sidebands and $\sim 10\%$ of coincidence background, were subtracted with the appropriate weights. The mass resolution was limited by the uncertainties in the transfer matrix. For the Λ hyperons, events were selected in the range $1.110 < M_X\ [\mathrm{GeV}/c^2] < 1.140$, and for the Σ^0 hyperons, events were selected in the range $1.185 < M_X\ [\mathrm{GeV}/c^2] < 1.220$.

3 Cross-sections

The experimental kaon yield, Y_K, in the two channels can be related to the cross-section by

$$Y_K = \int \mathcal{L}\mathrm{d}t \times \frac{\mathrm{d}\sigma_v}{\mathrm{d}\Omega_K^{c.m.}} \times \int \Gamma(Q^2, W)\, f(Q^2, W)\, A\, R\, \mathrm{d}V, \quad (2)$$

where Γ is dependent on purely electromagnetic properties and can be considered as a "flux of virtual photons", so that the virtual photoproduction cross-section, σ_v, could be extracted. $\mathcal{L}$ is the experimental luminosity that includes global efficiencies such as dead times and beam current-dependent corrections such as the tracking efficiency. A is the acceptance function of the coincidence spectrometer setup, R is the correction due to radiative and energy losses, and $\mathrm{d}V$ the phase-space element. The accumulated and corrected luminosity in 2009 was $\int \mathcal{L}\mathrm{d}t \sim 2300\,\mathrm{fbarn}^{-1}$. The kaon sample collected in 2008 was taken with a beam current of only $0.5\,\mu$A and for a shorter time period. In a Monte Carlo simulation of the experiment, the phase-space integral was evaluated in the volume $\Delta V = \Delta Q^2 \Delta W \Delta\phi_e \Delta\Omega_K^{c.m.}$ with limits that extended beyond the physical acceptances of the spectrometers. Radiative corrections in R were included according to [20]. The solid angle acceptances for the electrons and kaons in the laboratory system were $\Omega_{e'}^{lab} = 5.6\,\mathrm{msr}$ and $\Omega_K^{lab} = 10.4\,\mathrm{msr}$. The acceptance in ϕ was flat ranging from $-15°$ to $+15°$ centred at $\langle\phi\rangle = 0$. The two different kaon momenta associated to Λ and Σ^0 hyperons were simultaneously within the momentum acceptance of the Kaos spectrometer.

The geometrical acceptance of the spectrometer setup, the path length from the target to the detectors, kaon decay in flight, and kaon multiple scattering were determined using the simulation package Geant4. The kaon survival fraction varied between 0.2 and 0.35 for the range of momenta detected. Fiducial cuts were applied to the target acceptance to restrict events to a region where agreement between the Monte Carlo code and the analysed data was excellent.

To study the dependence of the measured cross-section on the kaon centre-of-mass (c.m.) angle, $\cos\theta_K^{c.m.}$, the data were scaled to the centre of the electron-arm acceptance through the introduction of a scaling function $f(Q^2, W)$ inside the phase-space integral. The scaling minimized the effects of non-uniform distribution within the W and Q^2 bins and the extracted cross-sections can be accurately compared directly to theoretical calculations at the centre of each bin value. The scaling was performed with the predictions from isobaric models, see the next section for their description. The magnitude of the scaling varied between 0.85 and 1.15 with most of the events being scaled by less than 5%. The studied isobar models predicted only small variations of the scaling function. The model dependence and the uncertainty introduced by the scaling were included in the estimate of the systematic uncertainties.

At each kinematic setting, data were partitioned into several runs. The run-to-run variation of quantities like dead time, background particle yields, etc., was used as a consistency check. The systematic uncertainty assigned to the absolute cross-sections is 8% and is dominated by the uncertainties in Kaos acceptance (5%), MWPC tracking efficiencies (4%), analysis cut efficiencies (3%) and scaling model variation (2%). The beam current was measured on the 1% level. Other studied sources of systematic uncertainties included kaon survival probability, kaon decay particle misidentification, effective target length and target density fluctuations that introduced a systematic uncertainty on the percent level. These uncertainties were significantly smaller than the statistical uncertainties, which were in the range of 10–25%.

The elementary kaon electroproduction cross-section was measured at MAMI in a kinematic region of low Q^2 not covered by previous experiments. The measured angular differential cross-sections at $W = 1.75\,\mathrm{GeV}$ and $\langle Q^2\rangle = 0.036\,(\mathrm{GeV}/c)^2$ in the $K^+\Lambda$ and $K^+\Sigma^0$ reaction channels are shown in fig. 4. The magnitude of the cross-section is comparable to photoproduction data from the SAPHIR [21] and CLAS [13,16] measurements. Its angular dependence is almost flat in the $K^+\Sigma^0$ channel whereas in the $K^+\Lambda$ channel the data reveals a moderate angular dependence, which is consistent with the photoproduction data and with conclusions drawn from the CLAS electroproduction data [14]. In fig. 5 the differential cross-section at larger momentum transfer $\langle Q^2\rangle = 0.050\,(\mathrm{GeV}/c)^2$ and smaller hadronic energy $\langle W\rangle = 1.67\,\mathrm{GeV}$ in the $K\Lambda$ channel is shown.

The cross-section data in the two hyperon channels are also compared to predictions from variants of the K-Maid model [6] and from the Saclay-Lyon [4] and Regge-plus-resonance [10,11] models. For the electromagnetic kaon production in the so-called third-resonance region, many resonances contribute, which presently cannot be described uniquely by a single model. The nomenclature for characterizing nucleon resonances is $L_{2I;2J}(M)$, where L is the orbital angular momentum of the partial wave, I is the isospin, J is the spin and M is the mass of the resonance.

The K-Maid model includes the kaon resonances $K^*(890)$ and $K_1(1270)$ in the t-channel, as well as four nucleon resonances, $S_{11}(1650)$, $P_{11}(1710)$, $P_{13}(1720)$, and the "missing" resonance $D_{13}(1895)$ included to shape a

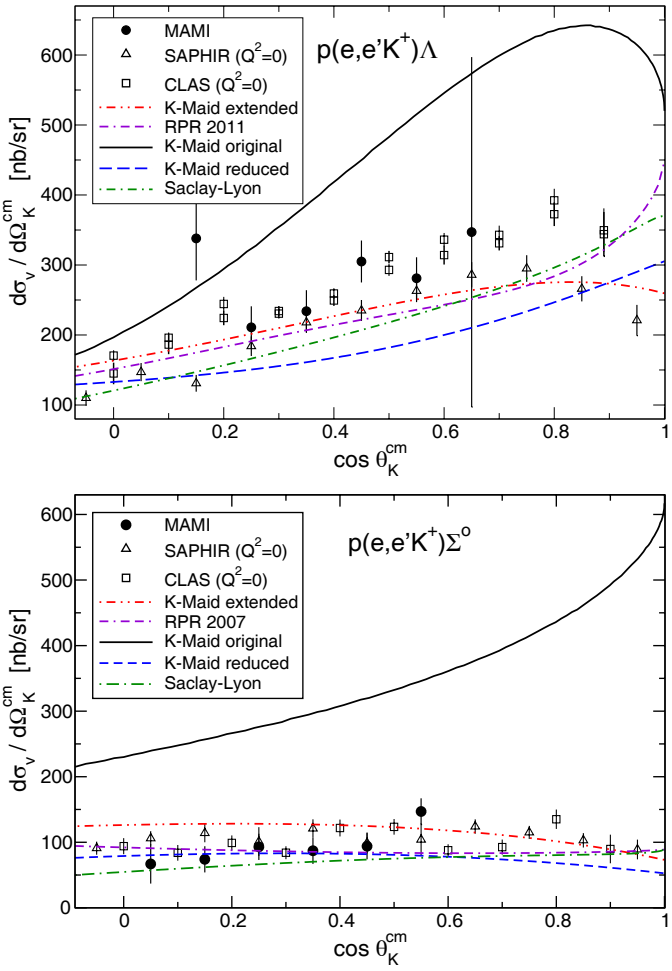

Fig. 4. Differential cross-sections of kaon electroproduction scaled to the centre of the experimental acceptance at $\langle Q^2\rangle = 0.036\,(\mathrm{GeV}/c)^2$, $\langle W\rangle = 1.75\,\mathrm{GeV}$ and $\langle\varepsilon\rangle = 0.4$. The MAMI data are compared to variants of the K-Maid model [6] (see the text for discussion on the variations), the Saclay-Lyon model [4], and the Regge-plus-resonance model [10,11]. The K-Maid and Saclay-Lyon model predictions were averaged in Q^2 between 0.030–0.045 $(\mathrm{GeV}/c)^2$ and in W between 1.74–1.76 GeV. The predictions from the Regge-plus-resonance model variant RPR 2011 [11] and the variant RPR 2007 [10] are shown for the $K^+\Lambda$ and $K^+\Sigma^0$ channels, respectively. The photoproduction cross-sections at $Q^2 = 0$ are from the SAPHIR experiment at $W = 1.757\,\mathrm{GeV}$ [21] and from the CLAS experiment at $W = 1.745$ and $1.755\,\mathrm{GeV}$ [13,16].

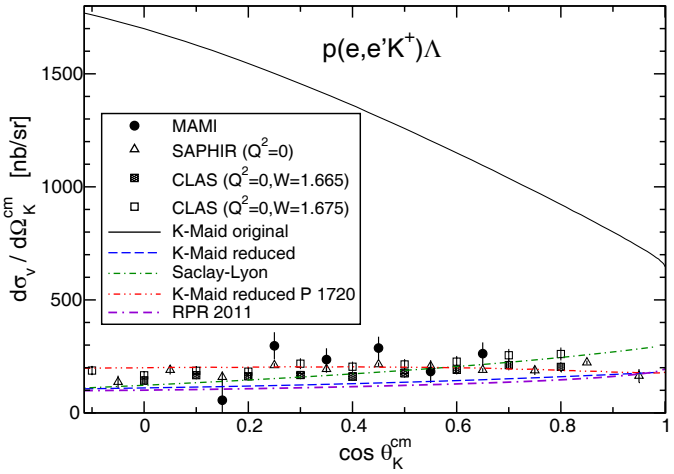

Fig. 5. Differential cross-sections of kaon electroproduction scaled to the centre of the experimental acceptance at $\langle Q^2\rangle = 0.05\,(\mathrm{GeV}/c)^2$, $\langle W\rangle = 1.67\,\mathrm{GeV}$ and $\langle\varepsilon\rangle = 0.54$. The data are compared to variants of the K-Maid model [6] (see the text for discussion on the variations), the Saclay-Lyon model [4], and the Regge-plus-resonance model [11]. The photoproduction cross-sections at $Q^2 = 0$ are from the SAPHIR experiment [21] and from the CLAS experiment at $W = 1.665$ and $1.675\,\mathrm{GeV}$ [13,16].

structure around $W \approx 1.9\,\mathrm{GeV}$ in the cross-section of the $K^+\Lambda$ production. For $K^+\Sigma$ production the $D_{13}(1895)$ is replaced by the $S_{31}(1900)$ and $P_{31}(1910)$ Δ-resonances. No hyperon resonances are used in this model. Phenomenological form factors at the hadron vertices are used as a mechanism to counterbalance too large strength arising from point-like Born terms [7]. The cut-off parameters are fitted to data to account for the behaviour of the cross-sections in the high-energy region above $W > 1.9\,\mathrm{GeV}$ [6]. An interactive version of the model is available through the Internet [22] and is referred to in this paper as the original variant. In an extension of the model to the electroproduction process, the phenomenological electromagnetic form factors were added and the longitudinal couplings of the virtual photon to baryons were assumed. The longitudinal coupling constants, which cannot be established from the photoproduction data, were fitted using the Q^2 dependence between 0.52 and 2.0 $(\mathrm{GeV}/c)^2$ of the longitudinal and transverse structure functions measured at Jefferson Lab, where a steep rise of the longitudinal structure function towards lower Q^2 was found [23]. This model describes reasonably well also the data from the revised analysis by Mohring *et al.* [12] as well as other older electroproduction data, see, *e.g.*, figs. 3 and 4 in [24].

Another variant of the K-Maid model has been constructed, in which the strong longitudinal couplings to the nucleon resonances were removed to demonstrate the influence of the longitudinal couplings in the model predictions. In the variant labelled "P1720" only the longitudinal coupling to the $P_{13}(1720)$ nucleon resonance has been removed as this resonance is near to the investigated region at $W = 1.67$–$1.75\,\mathrm{GeV}$. Further, the same computer code as for the Saclay-Lyon model was used making results of the models fully mutually consistent. Analogous results obtained from the interactive version [22] revealed only minor differences. This variant of the K-Maid model is referred to in this paper as the reduced variant.

Finally, a new version of K-Maid is under construction, that uses very small longitudinal couplings [25]. In this version four nucleon resonances, $D_{15}(1675)$, $D_{13}(1700)$, $F_{15}(2000)$, and $D_{15}(2200)$ were added to those assumed in the original version and the free parameters of the model were refitted to describe polarized and unpolarized cross-sections from [21,13,14,26–28] on the photo- and electro-

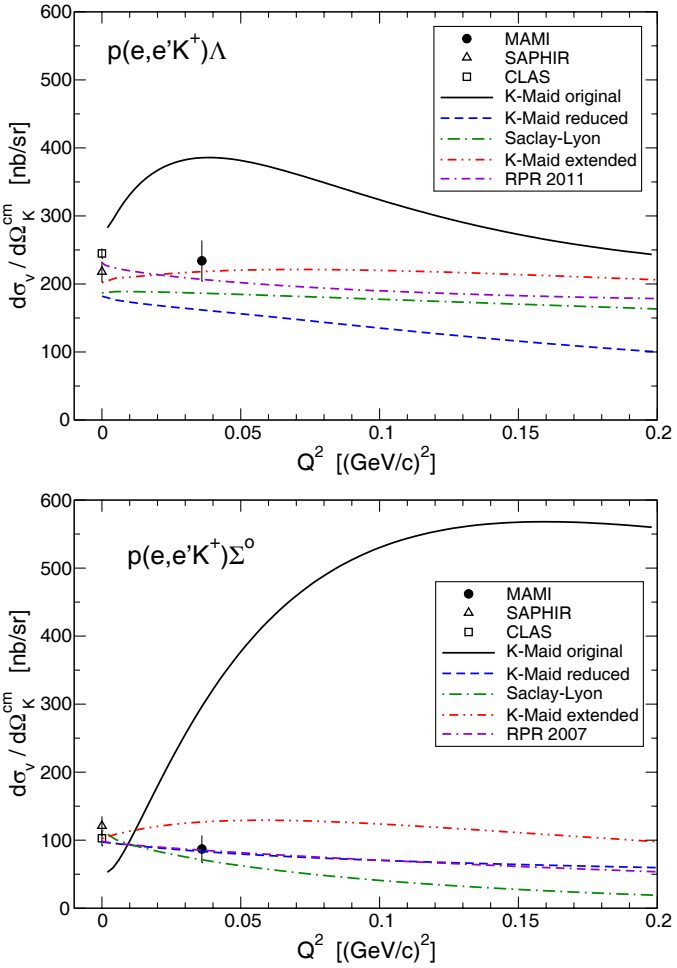

Fig. 6. Predictions for the dependence of the kaon electroproduction cross-sections on the virtual photon's four-momentum Q^2 at $\cos\theta_K^{c.m.} = 0.35$ and $W = 1.75\,\mathrm{GeV}$ compared to the two experimental data points from MAMI for the $K^+\Lambda$ and $K^+\Sigma^0$ reaction channels. References for models and data are the same as for fig. 4.

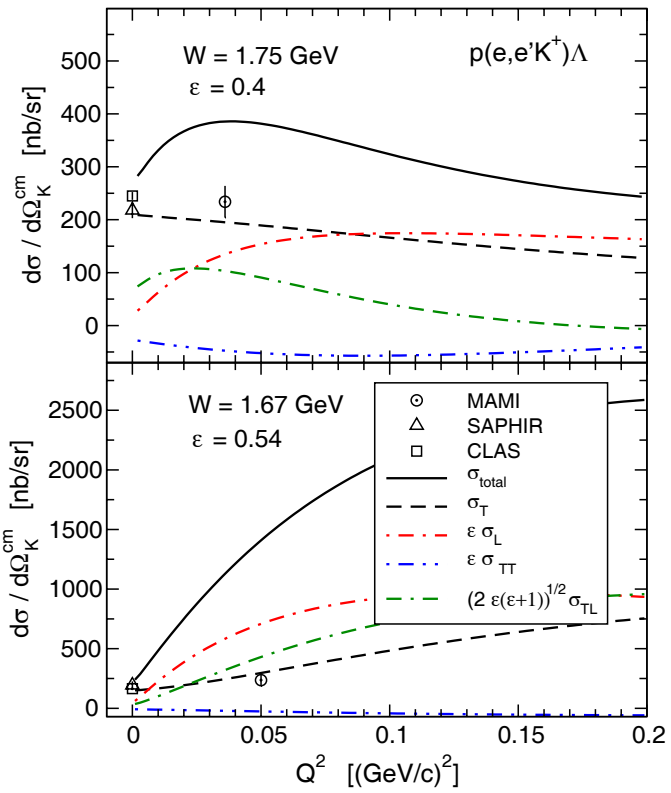

Fig. 7. Predictions from the original K-Maid model for the dependence of the kaon electroproduction cross-sections on Q^2 at $\cos\theta_K^{c.m.} = 0.35$, separated according to eq. (1), compared to the data from MAMI for the $K^+\Lambda$ reaction channel. A strong rise with Q^2 of the longitudinal, σ_L, and the transverse-longitudinal interference, σ_{TL}, structure functions was predicted by the model, especially at $W = 1.67\,\mathrm{GeV}$ where the influence of a strong longitudinal coupling of the resonance $P_{13}(1720)$ is apparent. In contrast, the transverse structure function, σ_T, is only slowly varying with Q^2. References for model and data are the same as for fig. 4.

production of kaons [25]. This version is referred to as the extended variant.

The Saclay-Lyon model shares with K-Maid the same kaon resonances and the broken $SU(3)$ symmetry constraints on the main coupling constants. The set of nucleon resonances differs from K-Maid and includes resonances with spins up to $5/2$, see [4]. Instead of hadronic form factors the spin-$1/2$ hyperon resonances $S_{01}(1405)$, $P_{11}(1660)$, $S_{01}(1670)$ and $P_{01}(1810)$ are used for counterbalancing the strength of the Born terms through a destructive interference with these u-channel resonances. For $K^+\Sigma^0$ production, the $P_{33}(1232)$, $P_{31}(1910)$, and $P_{33}(1920)$ Δ-resonances are added to those given above. No longitudinal couplings are included in this model. This model is successful in predicting correct cross-sections for electroproduction of hypernuclei at very low Q^2 [29,30].

In the Regge-plus-resonance model for the $K\Lambda$ production the background is described by a Regge model in which two strongly degenerate kaon trajectories, $K^+(494)$ and $K^{*+}(892)$, are exchanged. The coupling constants were fitted to CLAS data [16] for energies $2.6 < W < 3\,\mathrm{GeV}$. The resonance part of the amplitude includes contributions from exchanges of the nucleon resonances $S_{11}(1535)$, $S_{11}(1650)$, $F_{15}(1680)$, $P_{13}(1720)$, $D_{13}(1900)$, $P_{13}(1900)$, $P_{11}(1900)$, and $F_{15}(2000)$, which is a result of robust and very careful analysis of data on $K^+\Lambda$ photoproduction in the resonance region ($W < 2.6\,\mathrm{GeV}$). These s-channel contributions are regularized beyond the resonance pole assuming spin-dependent multidipole-Gauss hadronic form factors. In the extrapolation of the RPR model for non-zero Q^2, monopole electromagnetic form factors were added to the trajectories and the transition form factors in the resonance exchanges were described by the Bonn constituent quark model [11]. The longitudinal couplings are neglected in the RPR model. The variant "RPR 2011" of the model is optimised for the full range of kaon angles in contrast to the variant "RPR

2007" [10], which was constructed for kaon angles in the forward hemisphere.

4 Discussion

The electroproduction cross-section near the photoproduction point is very important for understanding the dynamics of the process. The MAMI data indicate a smooth transition in Q^2 from photoproduction to electroproduction cross-sections for both reaction channels as shown in fig. 6. The CLAS data on the unpolarized cross-section in the $K^+\Lambda$ channel, measured for $0.65 < Q^2 < 2.5\,(\mathrm{GeV}/c)^2$, reveals a fall off with respect to the photoproduction point [14]. However, the extrapolation of this trend to the photoproduction point with a dipole form results in a too large structure function σ_T [14], which is apparent especially at forward kaon angles. These observations suggest a more complex dynamics of the $K^+\Lambda$ electroproduction process in the transition region of $0 < Q^2 < 0.5\,(\mathrm{GeV}/c)^2$.

Information could also be obtained on the electromagnetic couplings to hadronic resonances. In fig. 7 separated cross-sections from the original K-Maid model are compared to the MAMI data which covers a range in Q^2 from 0.030 to $0.055\,(\mathrm{GeV}/c)^2$. It was predicted that the longitudinal contribution exceeded the transverse cross-section which was explained in the model by a strong longitudinal coupling of the electromagnetic field to the resonances. These couplings are given in the Lagrangian at the nucleon-photon–resonance vertices by a term that is proportional to Q^2. This effect is apparent especially in fig. 7 at $W = 1.67\,\mathrm{GeV}$ where the steep rise of the longitudinal cross-sections is due to the contribution from a strong longitudinal coupling of the resonance $P_{13}(1720)$. In contrast, models without longitudinal couplings predicted the electroproduction cross-sections below the photoproduction data, which means that in these variants the total cross-section slowly varied with momentum transfer. Also, the extended variant of the K-Maid model reveals a rather flat dependence of the cross-section in both channels on the momentum transfer.

This first open strangeness experiment has also demonstrated that the Kaos spectrometer is, in connection with the high-quality continuous wave electron beam of MAMI, a very effective tool for investigating kaon production off nucleons and nuclei with electron scattering. Based on the MAMI data some versions of isobar models for the process, which assumed strong longitudinal couplings to the nucleon resonances, could be excluded at the low energies that were probed. Other models, in which weak or no longitudinal couplings to N^* resonances appear, predict much smaller total cross-sections and are in better agreement with the data. At MAMI, new measurements at very low Q^2 with polarized beam and much higher statistical significance will provide more complete information on this process and therefore will deliver additional new constraints on the model parameters.

To conclude, this measurement and expected new data from MAMI in this kinematic region will help in better understanding the dynamics of the electromagnetic kaon production and in the modelling of the nucleon and its resonances.

We would like to thank the accelerator group of MAMI and the staff of the workshops for their excellent support. We are thankful to T. Mart from the University of Indonesia for providing the K-Maid code and assisting in the interpretation of the model and to L. De Cruz for providing us results for the RPR model. We also thank Th. Walcher and A. Jankowiak for their support in the early phase of the project. Work supported in part by the Federal State of Rhineland-Palatinate and by the Deutsche Forschungsgemeinschaft (DFG) with the Collaborative Research Center 443, by the Research Center "Elementary Forces and Mathematical Foundations", and by the DFG with the HBFG-122-572 grant. We also acknowledge the support by the Research Infrastructure Integrating Activity "Study of Strongly Interacting Matter" HadronPhysics2 under the 7th Framework Programme of EU and by the Grant Agency of the Czech Republic, grant No. 202/08/0984.

References

1. K.H. Kaiser *et al.*, Nucl. Instrum. Methods Phys. Res. A **593**, 159 (2008).
2. R.A. Adelseck, B. Saghai, Phys. Rev. C **42**, 108 (1990).
3. R.A. Williams, C.R. Ji, S.R. Cotanch, Phys. Rev. C **46**, 1617 (1992).
4. J.C. David, C. Fayard, G.H. Lamot, B. Saghai, Phys. Rev. C **53**, 2613 (1996).
5. T. Mizutani, C. Fayard, G.H. Lamot, B. Saghai, Phys. Rev. C **58**, 75 (1998).
6. T. Mart, C. Bennhold, Phys. Rev. C **61**, 012201 (2000).
7. S. Janssen, J. Ryckebusch, D. Debruyne, T. Van Cauteren, Phys. Rev. C **65**, 015201 (2002).
8. R. Shyam, O. Scholten, H. Lenske, Phys. Rev. C **81**, 015204 (2010).
9. B. Juliá-Diaz, B. Saghai, T.S.H. Lee, F. Tabakin, Phys. Rev. C **73**, 055204 (2006).
10. T. Corthals, D.G. Ireland, T. Van Cauteren, J. Ryckebusch, Phys. Rev. C **75**, 045204 (2007).
11. L. De Cruz, T. Vrancx, P. Vancraeyveld, J. Ryckebusch, *Bayesian inference of the resonance content of* $p(\gamma, K^+)\Lambda$, arXiv:1111.6511 [nucl-th] (2011).
12. E93-018 Collaboration (R.M. Mohring *et al.*), Phys. Rev. C **67**, 055205 (2003).
13. CLAS Collaboration (R. Bradford *et al.*), Phys. Rev. C **73**, 035202 (2006).
14. CLAS Collaboration (P. Ambrozewicz *et al.*), Phys. Rev. C **75**, 045203 (2007).
15. Hall A Collaboration (M. Coman *et al.*), Phys. Rev. C **81**, 052201 (2010).
16. CLAS Collaboration (M.E. McCracken *et al.*), Phys. Rev. C **81**, 025201 (2010).
17. A1 Collaboration (K.I. Blomqvist *et al.*), Nucl. Instrum. Methods Phys. Res. A **403**, 263 (1998).
18. A1 Collaboration (P. Achenbach *et al.*), Eur. Phys. J. ST **198**, 307 (2011).
19. A1 Collaboration (P. Achenbach *et al.*), Nucl. Instrum. Methods Phys. Res. A **641**, 105 (2011).
20. L.W. Mo, Y.S. Tsai, Rev. Mod. Phys. **41**, 205 (1969).

21. SAPHIR Collaboration (K.H. Glander *et al.*), Eur. Phys. J. A **19**, 251 (2004).
22. T. Mart, C. Bennhold, H. Haberzettl, L. Tiator, *An effective Lagrangian model for kaon photo- and electroproduction on the nucleon*, available online at `www.kph.uni-mainz.de/MAID/kaon/kaonmaid.html`.
23. E93-018 Collaboration (G. Niculescu *et al.*), Phys. Rev. Lett. **81**, 1805 (1998).
24. P. Bydžovský, F. Cusanno, S. Frullani, F. Garibaldi, M. Iodice, M. Sotona, G.M. Urciuoli, *Models for photo- and electro-production of K^+ in view of new data*, arXiv:nucl-th/0305039 (2003).
25. T. Mart, L. Tiator, private communication (2011).
26. CLAS Collaboration (R. Bradford *et al.*), Phys. Rev. C **75**, 035205 (2007).
27. CLAS Collaboration (R. Nasseripour *et al.*), Phys. Rev. C **77**, 065208 (2008).
28. CLAS Collaboration (D.S. Carman *et al.*), Phys. Rev. C **79**, 065205 (2009).
29. Hall A Collaboration (M. Iodice *et al.*), Phys. Rev. Lett. **99**, 052501 (2007).
30. Hall A Collaboration (F. Cusanno *et al.*), Phys. Rev. Lett. **103**, 202501 (2009).